

RESEARCH ARTICLE

Targeting caveolae to pump bispecific antibody to TGF- β into diseased lungs enables ultra-low dose therapeutic efficacy

Anil H. Kadam¹, Kathirvel Kandasamy¹, Tim Buss¹, Brittany Cederstrom¹, Chun Yang¹, Sreekanth Narayanapillai¹, Juan Rodriguez¹, Michael D. Levin¹, Jim Koziol¹, Bogdan Olenyuk¹, Zea Borok², Adrian Chrastina¹, Jan E. Schnitzer^{1,3*}

1 Proteogenomics Research Institute for Systems Medicine (PRISM), La Jolla, California, United States of America, **2** Department of Medicine, UCSD School of Medicine, La Jolla, California, United States of America, **3** Institute for Engineering in Medicine, UCSD, La Jolla, California, United States of America

* JSchnitzer@prism-sd.org



OPEN ACCESS

Citation: Kadam AH, Kandasamy K, Buss T, Cederstrom B, Yang C, Narayanapillai S, et al. (2022) Targeting caveolae to pump bispecific antibody to TGF- β into diseased lungs enables ultra-low dose therapeutic efficacy. PLoS ONE 17(11): e0276462. <https://doi.org/10.1371/journal.pone.0276462>

Editor: You-Yang Zhao, Ann and Robert H Lurie Children's Hospital of Chicago, Northwestern University, UNITED STATES

Received: June 15, 2022

Accepted: October 6, 2022

Published: November 22, 2022

Copyright: © 2022 Kadam et al. This is an open access article distributed under the terms of the [Creative Commons Attribution License](https://creativecommons.org/licenses/by/4.0/), which permits unrestricted use, distribution, and reproduction in any medium, provided the original author and source are credited.

Data Availability Statement: All relevant data are within the manuscript and its [Supporting Information](#) files.

Funding: This study was supported by the National Institutes of Health (<https://www.nih.gov/grants-funding>) through grants awarded to JES (P01HL119165 and P01CA221775). The funders had no role in study design, data collection and

Abstract

The long-sought-after “magic bullet” in systemic therapy remains unrealized for disease targets existing inside most tissues, theoretically because vascular endothelium impedes passive tissue entry and full target engagement. We engineered the first “dual precision” bispecific antibody with one arm pair to precisely bind to lung endothelium and drive active delivery and the other to precisely block TGF- β effector function inside lung tissue. Targeting caveolae for transendothelial pumping proved essential for delivering most of the injected intravenous dose precisely into lungs within one hour and for enhancing therapeutic potency by >1000-fold in a rat pneumonitis model. Ultra-low doses ($\mu\text{g}/\text{kg}$) inhibited inflammatory cell infiltration, edema, lung tissue damage, disease biomarker expression and TGF- β signaling. The prodigious benefit of active vs passive transvascular delivery of a precision therapeutic unveils a new promising drug design, delivery and therapy paradigm ripe for expansion and clinical testing.

Introduction

Modern medicine seeks precision in diagnosis and therapy. Ehrlich's ideal of “aiming precisely” using drugs remains a challenge [1–6]. Molecular medicine has advanced to achieve unparalleled interactive specificity in the high affinity binding of imaging and therapeutic agents. But this target binding precision does not automatically translate into the low dose therapeutic efficacy expected with high specific affinity. Many antibodies and other drugs designed to precisely target a therapeutic moiety expressed inside key diseased organs like lung actually do so below theoretical expectation after systemic administration [2–6]. Targeting and molecular imaging are slow, inefficient and not particularly specific. Frequently it is not the target choice nor binding specificity or affinity but rather poor access that is limiting precision-targeted therapies *in vivo*.

analysis, decision to publish, or preparation of the manuscript.

Competing interests: The authors have declared that no competing interests exist.

A thin monolayer of endothelial cells (ECs) lining the inner surface of all blood vessels physically separates drugs circulating in the blood from tissue cells [3, 4]. Systemic therapeutics must frequently overcome this major biological barrier to gain target access inside key organs and attain effective concentrations locally at the disease site. Currently all drugs depend on passive transvascular transport, primarily by diffusion and hydraulic drag through intercellular EC junctions or gaps, to reach and bind their targets inside tissue [4–6]. Nonspecific and inefficient penetration of solid tissues necessitates high, sometimes near toxic doses to drive enough drug uptake to realize therapeutic efficacy. The current passive drug delivery paradigm appears to likely limit both therapeutic potency and efficacy while promoting undesired on- and off-target adverse effects elsewhere in the body [2–6].

Advances in genetic antibody engineering in the last few years have permitted designing a whole new generation of bi- and multi-specific antibodies to address the unmet medical need for better targeting and therapeutic precision without deleterious side effects. In theory dual binding can improve tissue targeting and therapeutic potency, efficacy and index of standard monospecific antibodies. But bispecifics still rely on passive delivery and thus have achieved their biggest gains so far in treating hematogenous disease where therapeutic targets are inherently more accessible. Lowering doses could benefit patients by minimizing toxicities usually seen at high doses and improving greatly the therapeutic index. In many cases, we don't know whether drugs have achieved optimal concentration for maximum therapeutic effect, and we have to wonder, when drugs fail, whether they reached the target, especially inside solid tissue, at the necessary concentration to get full impact. Given that modern drugs are so well made and tested for maximal pharmacological activity, then with proper delivery assured the target must be lacking, for instance in expression homogeneity or in driving the pathology. Here we engineer a bispecific quad antibody format to create the first precision therapeutic to go beyond passive transvascular transport into a solid tissue, the lung.

Our group discovered an alternative and promising, active and specific, caveolae-mediated transcytotic mechanism in endothelium *in vivo* [7–10]. We established that caveolae are not just static invaginations but can actually be dynamic transport vesicles with the molecular machinery for vesicular fission and fusion [11–15] necessary to carry and even pump select molecular cargo across microvascular endothelium. Proteomic mapping of the EC luminal surface and caveolae revealed apparent tissue-specific targets [8]. Ultimately our imaging studies including intravital fluorescence microscopy of lung showed that select imaging probes, only when binding a target highly concentrated in lung EC caveolae, such as aminopeptidase P2 (APP2), can be transported rapidly across the EC barrier to concentrate solely in the lung interstitium within minutes of intravenous (iv) injection; this extravasation continued even against a concentration gradient which by definition constitutes active transport or pumping [7, 10].

Although clearly promising in theory, whether and to what degree targeting this caveolae-mediated transendothelial pumping system can help solve the long-standing drug delivery problem remains debatable. How much the EC barrier contributes on its own is unknown. Can an authentic precision therapeutic with remarkable high affinity and documented efficacy benefit from active delivery and in what way and how much? Here, we begin to answer these critical questions and discover and quantify a striking therapeutic impact.

We exploit the active precision delivery portal for possible therapeutic utility by genetically engineering a new antibody class, the first bispecific quad antibody where two arms enable active transvascular delivery into a normally restrictive solid tissue so that the second pair of arms can block the therapeutic target deep inside the solid tissue. We recombinantly engineer this “dual precision” therapeutic to combine key binding domains of a precision therapeutic antibody specifically neutralizing transforming growth factor- β (TGF- β) effector function with a precision lung-targeting and penetrating antibody specific for APP2. Testing the effects of

active vs passive transvascular delivery on a precision therapeutic is now possible for the first time.

TGF- β regulates inflammatory and tissue remodeling responses that direct many acute and chronic pathologies in lung and other organs [16–20]. Inhibiting TGF- β with small molecules and antibodies shows impressive potency in treating many diseases including lung diseases ranging from acute respiratory distress syndrome (ARDS) to chronic fibrosis [21–25] and quite recently COVID-19 [26–28]. But effective treatment requires repeated high doses (mg/kg) that can elicit significant on- and off-target tissue side effects, including cardiovascular toxicity, bleeding, and death [29–32]. TGF- β 's pleiotropic functions and widespread tissue expression enables further consequences from disrupted TGF- β signaling: pathogenic immune response, cancer, abnormal wound healing, neurodegenerative diseases, pulmonary hypertension and renal and cardiac fibrosis [33]. Here we attempt to render lung targeting precision to a TGF- β blocking antibody for treating lung disease.

Materials and methods

Animals

Female Sprague Dawley rats (ENVIGO, USA) weighing 200–220 g were housed at 25°C with a 12 h day/night cycle and food and water *ad libitum*. Animals were maintained under these conditions until the end of the study. Care and experiments were approved by the PRISM Institutional Animal Care and Use Committee.

Antibodies and reagents

Recombinant rat aminopeptidase 2 (APP2) as well as recombinant antibodies fresolimumab, 833c, 833c&Freso and 833cX&Freso were genetically engineered in-house.

833c&Freso genetic engineering and characterization

833c is a chimeric antibody with murine variable regions (VH and Vk) and human constant regions (CH1-CH2-CH3 and Ck) [9]. The heavy chain of 833c&Freso was synthesized by attaching the single chain Fv fragment of human fresolimumab to the C-terminus of the human CH3 domain via a SGGGS linker. The whole cassette was cloned into the TOPO-TA cloning vector pcDNA3.4. The light chain was encoded by a separate pcDNA3.4 vector. Antibodies were transiently expressed in CHO-S cells using the Expifectamine transfection kit at a molar ratio of heavy to light chain plasmids of 1:1.2. ExpiCHO enhancer and feed were added on day 2. Cells were typically harvested on day 8 or 9 post transfection and removed from the culture by centrifugation. The supernatant was filtered through a 0.2 μ m sterile filter unit and antibody purified with a protein G Sepharose column (Cytiva HiTrap) on an AKTA purifier. Batch to batch stability was controlled using capillary isoelectric focusing.

Commercially available test kits and reagents

Rabbit anti-Phospho-Smad2 (Ser465/467)/Smad3 (Ser423/425) (D27F4), rabbit anti-Galectin-3/LGALS3, rabbit anti-Phospho-Akt (Thr308) (D25E6), rabbit-anti-Akt (pan) (C67E7), rabbit Phospho-p70 S6 Kinase (Thr389) (I08D2), rabbit anti-p70 S6 Kinase (49D7), rabbit anti-PDGFR Receptor β (28E1), and rabbit anti-GAPDH (D16H11) XP were purchased from Cell Signaling Technology (Danvers, MA). We used rabbit polyclonal anti-Fibronectin (ab2413) (Abcam, Cambridge, MA), recombinant hu TGF- β 1 (ProSci, Poway, CA), anti-TGF- β 1 IgY-Biotin (R&D Systems, Minneapolis, MN), anti-hIgG-HRP (Jackson ImmunoResearch Inc., West Grove, PA), 1D11 (Invitrogen) and goat anti-rabbit IgG-HRP (Thermo Fisher Scientific, Carlsbad, CA).

Rat Quantikine ELISA kit for TGF β 1, IL6, IL1 β , WISP-1, CINC-1 and TIMP-1 were purchased from R&D Systems (Minneapolis, MN).

The following reagents were used: Bleomycin, USP grade (Teva pharmaceuticals, North Wales, PA or Hospira pharmaceuticals, Lake Forest, IL), CHAPS hydrate and protease inhibitor cocktail (Sigma-Aldrich, St. Louis, MO), and phosphatase inhibitor cocktail II (Alfa Aesar, Tewksbury, MA). Nitrocellulose membrane filter paper sandwich (Invitrogen), Novex 8–16% Tris-Glycine-gel system (Invitrogen), SuperBlock™ (PBS) blocking buffer, 96-well flat-bottom microtiter plates, bovine serum albumin, 10X PBS pH = 7.4 (Gibco), HRP-conjugated streptavidin (Pierce), SuperSignal™ West Pico PLUS chemiluminescent substrate were purchased from Thermo Fisher Scientific (Carlsbad, CA). ABTS substrate (KPL, Maryland WA), TRIS-buffered saline (TBS, 10X) pH = 7.4 for western blot (Alfa Aesar, Tewksbury, MA) and 10% neutral buffered formalin (Leica biosystems, Buffalo Grove, IL) were used. Gel and western blot images were captured using a Konica Minolta Bizhub c284e scanner.

Rat APP2 binding assay

We coated 96-well flat-bottom plates with recombinant rat APP2 (5 μ g/ml) overnight at room temperature. After washing 3 times with PBS containing 0.05% Tween-20 (PBST), plates were blocked with PBS containing 1% BSA and 0.01% Tween-20 for 90 min. Serially diluted antibodies were added, and plates were incubated for 2 h, washed and incubated with anti-hIgG-HRP for 1 h. After final washing, ABTS substrate (100 μ l/well) was added for 15 min, and the reaction was terminated with 0.1 M citric acid, pH = 4.0 (100 μ l/well). Absorbance was read at 415 nm and results analyzed using GraphPad software.

TGF- β 1 binding assay

We coated 96-well plates with titrated antibody solutions (210.0–0.002 nM) overnight at 4°C. After washing and blocking, 100 μ l recombinant hu TGF- β 1 (50 ng/ml) was added and incubated at 37°C for 2 h. Plates were washed and incubated with 100 μ l anti-TGF- β 1 IgY-Biotin (1.0 μ g/ml) for 1 h. After washing, plates were incubated with HRP-streptavidin (1:2500). After final washes, ABTS substrate (100 μ l/well) was added for 15 min, the reaction terminated with 0.1 M citric acid, pH = 4.0 (100 μ l/well) and absorbance read at 415 nm. Results were analyzed using GraphPad software.

Bleomycin-induced acute lung injury

Bleomycin was dissolved in 1X PBS pH = 7.4. On day 0, rats were anesthetized with inhaled isoflurane (3%–5%) and received a single instillation intratracheally (it) of bleomycin (2 U/kg) using a 18 gauge needle attached to a 1 mL tuberculin syringe. Control animals received 300 μ l 1X PBS. After instillation, rats were allowed to recover from anesthesia and returned to their cages with free access to food and water. Animals were sacrificed on day 3, and acute lung injury relevant endpoints were analyzed.

Treatments with mono and bispecific antibodies

All antibodies were dissolved in 1X PBS pH = 7.4. 833c&Freso (1–100 μ g/kg), fresolimumab (10–3000 μ g/kg), 833c (10 μ g/kg) and 833cX&Freso (10 μ g/kg) were administered as a single dose iv through the tail either prophylactically one h prior to bleomycin challenge (-1 h), or on day 1 (D1) or day 2 (D2), or day 1 and day 2 (D1&2). Control animals received PBS. Animals were sacrificed on day 3 (D3).

SPECT/CT tomographic imaging

833c&Freso, 833cX&Freso, and fresolimumab were radiolabeled with iodine-125 (^{125}I) (PerkinElmer, Waltham, MA) using Pierce™ Iodination Beads (Thermo Fisher Scientific, Carlsbad, CA) according to the manufacturer's instructions, resulting in specific activities ranging from 5.5 $\mu\text{Ci}/\mu\text{g}$ to 13 $\mu\text{Ci}/\mu\text{g}$. Radiolabeling did not affect apparent K_d values as determined by ELISA. SPECT/CT imaging was performed using a nanoScan SPECT/CT imaging system (Mediso, USA). Rats were injected iv with the indicated amount of antibodies 24 h after bleomycin treatment, and SPECT/CT images were captured after 1 h and 24 h. Note that the 1 h timepoint is an average, because the imaging process takes about 30 to 90 min. Images were acquired for 60 sec/projection using a four head gamma camera with a rat-sized multi-pinhole. Images were collected in a 360° orbit with 60 s sampling every 6°. The pulse height analyzer window was >28.40 keV with a width of 20%. SPECT/CT reconstruction was performed using Nucline nanoScan software (Mediso, Arlington, VA). CT voltage was set at 50 Kv, exposure for 300 msec and 720 helical projections were captured. After CT/SPECT fusion, SPECT/CT 3-D data sets were processed with VivoQuant software (Invicro, Boston, MA). SPECT Planar imaging with ^{125}I -833c&Freso was done at 3 $\mu\text{g}/\text{animal}$.

Size-exclusion chromatography with multi angle light scattering detection (SEC-MALS)

Antibodies were concentrated to 2 mg/mL using Cytiva Vivaspin® 500 50kDa MWCO (Cytiva, United Kingdom) spin filters. A total volume of 50 μL was injected into an HPLC instrument (Nexera SIL-20AC XR autosampler (Shimadzu), Nexera LC-20AD XR pump (Shimadzu), WTC-030S5 size exclusion chromatography column (5 μM , 300 Å, 7.8 X 300 mm, Wyatt Technology, USA) stabilized at 25°C in a CTO-20AC column oven (Shimadzu), SPD-M20A diode array detector (Shimadzu) followed by MiniDawn TREOS light scattering and Optilab T-rEX refractive index detectors (Wyatt Technology, USA). The DLS signal was collected by the TREOS detector and processed by the DynaPro NanoStar detector (Wyatt Technology, USA). Separation was carried out under an isocratic flow at 0.5 ml/min of 150mM sodium phosphate buffer, pH 7.0. Data was processed using ASTRA® V 7.3 software (Wyatt Technology, USA).

In vivo biodistribution analysis

One or 2 days after bleomycin administration rats were injected iv with 3 or 10 μg radiolabeled antibodies. After 1 or 24 h, rats were euthanized. Blood and excised major organs were weighed, and radioactivity was measured on a Wizard 1470 Automatic Gamma counter (PerkinElmer Life Sciences, Wallac Oy, Finland). Radiation uptake is expressed as percentage of injected dose (% ID) and percentage of injected dose per gram of tissue (%ID/g). Tissue targeting index (TTI) was calculated as antibody per g of lung tissue/antibody per g of blood [10]. We observed no significant differences in results from day one or two and 3 or 10 μg , and data were pooled.

Bronchoalveolar lavage (BAL)

Three days after bleomycin instillation, animals were euthanized with Euthazol (100–120 mg/kg) by intraperitoneal injection. The trachea was exposed following a small incision to the skin and BAL was performed 3 times using a plastic cannula with 2 mL 1X PBS (pH = 7.4). Volumes of individual BAL aspirates were pooled.

Assessment of pulmonary inflammatory cells

We mixed equal volumes of BAL fluid (BALf) and Turk's solution and counted total leukocytes manually using a hemacytometer (Hausser Scientific, Horsham, PA). The remaining fluid was centrifuged at 4000 RPM for 5 min at 4°C, aliquots of BALf supernatant were collected aseptically and stored at -80°C until analysis. Cell pellets were reconstituted in rat serum and stained with Leishman solution on frosted glass slides (Leica Biosystems). Using a light microscope (BX2, Olympus, Tokyo, Japan) at 100X magnification 500 cells/slide were counted. Cells were categorized based upon morphology into neutrophils, lymphocytes, eosinophils, or macrophages.

Lung harvest for protein-, histology- and edema analysis

After BAL, right lungs were harvested from animals, washed in 1X PBS and stored at -80°C until western blot analysis. For histology, left lungs were carefully removed and stored in 10% neutral buffered formalin (NBF). Paraffin-embedded tissue (4 µm slides) was stained with haematoxylin and eosin. In a separate set of rats, lungs were harvested without performing BAL to determine the severity of pulmonary edema by the ratio of whole wet to dry weight. To obtain dry weight, lungs were incubated in an oven (45°C for 24 h).

Lung injury scoring criteria

Pathological changes in lung tissue were assessed using the following criteria which were adapted from previously published protocols [34–36]: 1. cell infiltration severity 0–4 (0: normal, 1: mild, 2: moderate, 3: severe, 4: highly severe), 2. presence and absence of hyaline membranes (0: absence and 1: presence), 3. presence and absence of pulmonary edema (0: absence and 1: presence), 4. alveolar septal thickening 0–3 (0: Normal, 1: 2X, 2: 3X, 3: >3x) in total 20 random microscopic fields (20X magnification). Lung injury scores reflect the sum of criteria above. Lung samples for histology were obtained from 3 different independent experiments (n = 2-3/group).

Quantification of biomarkers of inflammation in rat lungs

TGF-β, IL-6, IL-1β, WISP-1, CINC-1, and TIMP-1 levels in BALf were determined using rat Quantikine ELISA following manufacturer's instructions.

Lung preparation and western blot analysis

Lungs were placed in 1 ml PBS containing 0.1% (v/v) protease and phosphatase inhibitor cocktail and stored at -80°C until use. Lungs were homogenized on ice in 5 mL CHAPS buffer containing protease and phosphatase inhibitors using a homogenizer (PT3100-POLYTRON, Kinematica, NY). Homogenates were centrifuged at 15,000 rpm for 15 min at 4°C, and the supernatant was stored at -80°C until use. Total protein concentrations were determined using bicinchoninic acid (BCA) assay. Proteins (50 µg) were separated on Novex 4–12% Tris-Glycine gels, transferred onto nitrocellulose membranes, blocked with SuperBlock™ for 2 h at room temperature (RT) and incubated with primary antibodies diluted in TRIS buffered saline pH = 7.4 (TBS) containing 0.1% Tween-20 following manufacturer's instructions. After washing with TBS-Tween, membranes were incubated with goat anti-rabbit IgG HRP-linked secondary antibody (1:10,000) for 1 h at RT and proteins were visualized by enhanced chemiluminescence.

Statistical analysis

All data are presented as mean \pm S.D. Student's t test was performed for comparing 2 groups and one way ANOVA followed by Dunnett's multiple comparison test for more than 2 groups. Differences were considered statistically significant for $P < 0.05$ compared with bleomycin control.

Data and materials availability

All data are available in the main text or the supplementary materials.

Results

To ascertain the extent to which the EC barrier limits therapeutic impact and to overcome high dosing and poor lung-specific delivery, we generated a bispecific antibody by genetically splicing a single chain Fv (scFv) fragment of the TGF- β -neutralizing antibody fresolimumab onto the C-terminus of a lung-targeting APP2 chimeric antibody (833c) (Fig 1A and 1B). The two arms of the antibody, 833c and fresolimumab, were chosen to serve two distinct purposes; 833c to bind to EC caveolae and drive active delivery into the lung interstitium and fresolimumab to block TGF- β signaling pathways. This bispecific antibody 833c&Freso was expressed and purified up to 99% monomer (Fig 1C and 1D). Every batch of antibody was confirmed to be at least 97% pure. ELISA confirmed 833c&Freso maintained binding affinity to both targets (Fig 1E and 1F) unlike a mutated version 833cX&Freso, which did not bind APP2 by design

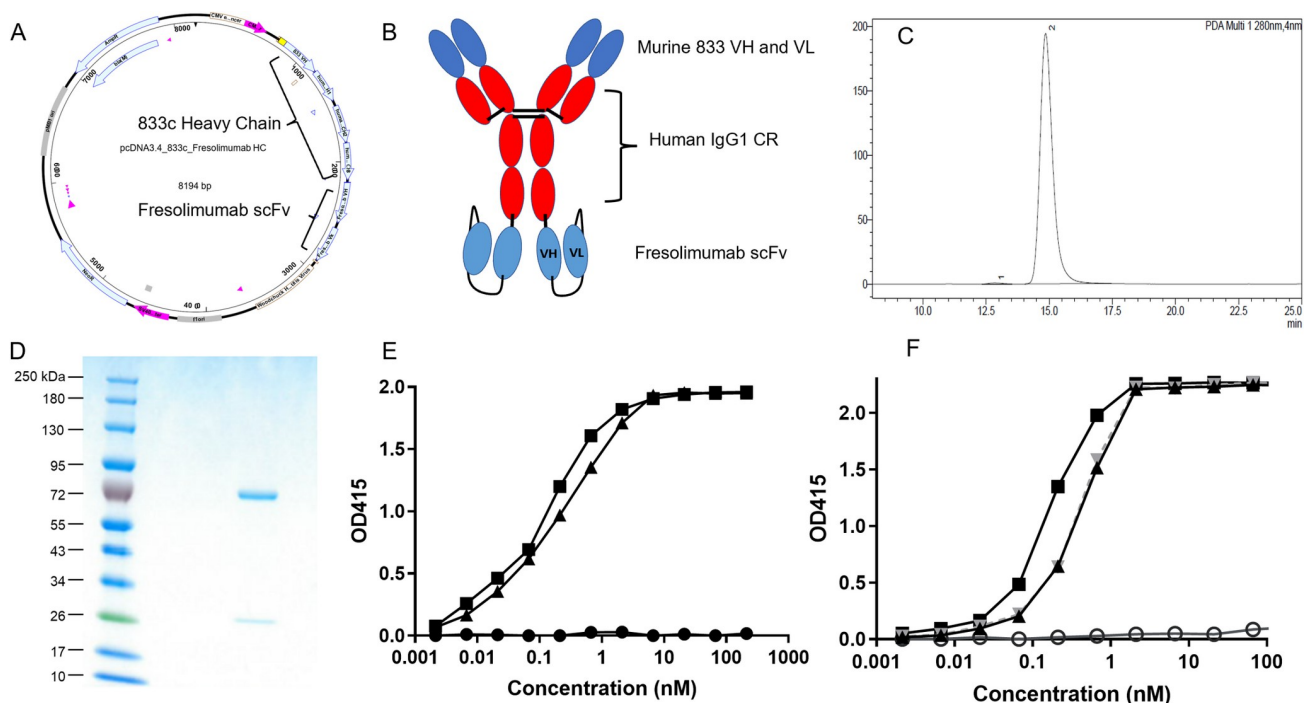


Fig 1. Genetic engineering and characterization of 833c&Freso. (A) Plasmid map for 833c&Freso heavy chain expression. Fresolimumab single-chain variable fragment (scFv) was cloned into the 3' end of the 833c CH3 domain. (B) 833c&Freso schematic: scFv is attached to the CH3 domain at the 3' end. Red: human domains, blue: murine domains. CR: constant region, VH and VL: variable regions. (C) Size exclusion chromatography and (D) Reducing SDS-PAGE of purified 833c&Freso. (E) ELISA binding to rat aminopeptidase P2 of 833c&Freso (triangles), 833cX&Freso (circles) and 833c (squares) (see Methods). (F) ELISA binding to TGF- β 1 of 833c&Freso (triangle, black), 833cX&Freso (triangle, gray), fresolimumab (squares) and huIgG4, a isotype-matched control IgG for fresolimumab (open circles) (see Methods).

<https://doi.org/10.1371/journal.pone.0276462.g001>

(see [Methods](#)). Size-exclusion chromatography with multi angle light scattering detection confirmed only a minimal increase in the average hydrodynamic radius of the bispecific antibody 833c&Freso (6.1 nm) and 833cX&Freso (6.1 nm) compared to 833c (5.2 nm) and fresolimumab (5.0 nM) ([S1 Fig](#)). Through recombinant engineering, we hope to have designed the first bispecific therapeutic to be pumped across the EC barrier to concentrate in the interstitium and engage its target deep inside a single solid tissue, in this case the lung. The delivery arms of the bispecific should by design attain the critical access for the therapeutic arms to reach and engage their target for utmost efficacy.

To test the therapeutic potential of this novel heterobifunctional antibody, we chose the clinically relevant bleomycin model. Bleomycin is used to treat cancer patients but can cause acute lung injury, fibrosis, ARDS and even death. In animal models, bleomycin is widely used to study lung inflammation and fibrosis [36]. The bleomycin lung injury model shares mechanisms, pathology and sequelae seen in COVID-19 patients [25, 37, 38].

First, we tested lung immunotargeting of our antibodies. We challenged rats intratracheally (it) with bleomycin (see [Methods](#)) and after 24 or 48 h injected ^{125}I -833c&Freso intravenously (iv). Whole body imaging showed similar robust lung uptake. Planar γ -scintigraphy and SPECT/CT in maximum intensity projection (MIP) as well as cross sections all revealed remarkably precise lung imaging, both 1 h and 24 h post injection ([Fig 2A and 2B](#)). Neither the mutant ^{125}I -833cX&Freso nor ^{125}I -fresolimumab, which both lack APP binding, targeted the lungs even after 24 h. They remained mostly in the blood and exhibited the expected non-specific blood distribution profile ([Fig 2C–2F](#)).

Biodistribution analysis of excised organs confirmed lung immunotargeting with ^{125}I -833c&Freso (64% of injected dose/g lung) and very low blood levels, all within 1 h ([Fig 2G](#)). Up to 83% of the total dose accumulated in the lungs. Blood clearance was very rapid in contrast to the other antibodies which just remained in the bloodstream, even after 24 h. As expected, dehalogenation of antibody facilitated obvious release of radioiodine with

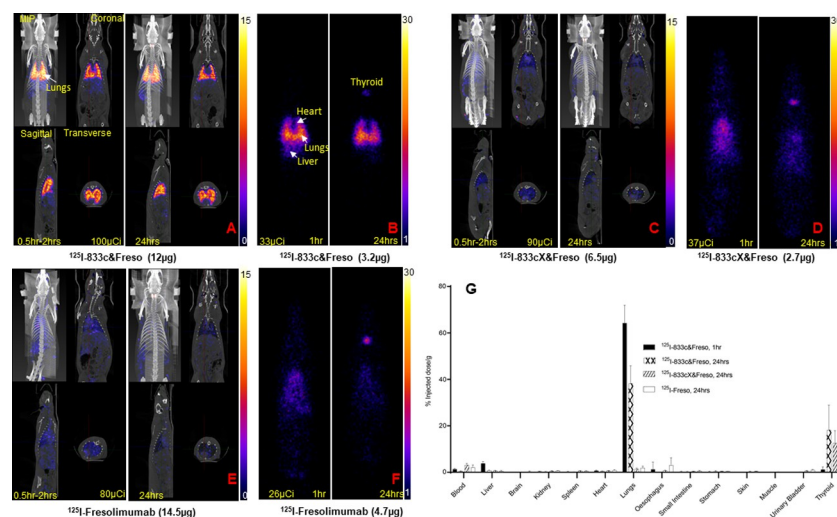


Fig 2. Lung targeting of 833c&Freso but not fresolimumab. After bleomycin treatment, rats were injected iv with radio-iodinated antibodies ^{125}I -833c&Freso, ^{125}I -833cX&Freso, and ^{125}I -fresolimumab (see [Methods](#)). (A, C, E) SPECT/CT images of rats taken at 1* and 24 h. Maximum intensity projection (MIP), coronal, sagittal, and transverse cross sections are shown. (B, D, F) Planar F067-scintigraphy imaging at the indicated timepoints. A-F: N = 2–3 rats per group (G) Biodistribution analysis of radioiodinated antibodies. Radioactivity was counted in the indicated organs excised from bleomycin-exposed rats. Uptake was quantified as the percentage of injected dose per gram tissue (means \pm SD). N = 3–10 rats per group. *Imaging started at 30 min and takes approximately 30 to 90 min.

<https://doi.org/10.1371/journal.pone.0276462.g002>

concomitant subsequent robust thyroid uptakes. Ultimately the two tissues with the most intense radioactive signal have a pumping mechanism: the lung via antibody transcytosis after APP2 binding in caveolae of lung ECs [7–10] and the thyroid through transmembrane pumping of freed radioiodine by the sodium-iodine symporter expressed in thyroid cells [39].

We quantified lung targeting precision by standard calculation of the tissue-targeting index (TTI) (antibody per g of lung tissue/antibody per g of blood) [10]. 833c&Freso produced an impressive TTI of 117 ± 31 (mean \pm SD) whereas the TTI was less than 1 for the other antibodies, consistent with their poor lung targeting. TTI comparison proved that adding APP2 binding to fresolimumab in this bispecific format did indeed improve lung targeting precision by over 100-fold.

We used these targeting data to inform dose selection for therapy. Fresolimumab binds to all three TGF β isoforms, but TGF- β 1 is predominantly induced during bleomycin lung pathogenesis [40]. Knowing the apparent affinity constant for antibody binding to APP2 (~ 0.2 nM) and fresolimumab to TGF- β 1 (1 nM) [31, 41, 42], we must attain a few fold higher concentration first in the blood to enable robust pumping by caveolae and then inside the lung tissue to achieve enough TGF- β blockade to render therapeutic efficacy. Our imaging injection of 3 μ g translates to ~ 15 μ g/kg dose; this generates peak blood levels above 1 nM, plenty for robust APP2 engagement and transport. With 70–80% delivered to the lung, we can attain ~ 10 nM inside the lungs which is more than enough to drive TGF- β engagement and blockade. Using half log progression, doses of 1, 3, 10, and 30 μ g/kg appeared warranted.

To assess pharmacological activity at μ g/kg doses in vivo, we first examined prophylactic efficacy by injecting 833c&Freso iv 1 h before bleomycin challenge. The effects of dose escalation were evaluated on the inflammatory cell profile in bronchoalveolar lavage fluid (BALf) harvested on day 3. Bleomycin greatly increased total leukocyte, neutrophil and lymphocyte levels from normally low to nil levels (S2 Fig). Rats treated with 833c&Freso doses above 3 μ g/kg showed statistically significant reductions in total leukocytes and neutrophils (S2 Fig).

We did not optimize these studies further but rather proceeded immediately to therapeutic testing. We selected day 2 post-bleomycin as most clinically relevant because bleomycin induced peak TGF- β 1 expression near day 2 (S3 Fig), the same day respiratory symptoms become clearly apparent. Again, total leukocyte and neutrophil levels were significantly reduced in animals receiving 1–30 μ g/kg 833c&Freso on day 2 (Fig 3A and 3B). 10 μ g/kg was statistically more effective than 1 μ g/kg but statistically indistinguishable from 3 and 30 μ g/kg. Inhibition of the bleomycin effect at 10 μ g/kg averaged 54% for leukocytes and 57% for neutrophils (Fig 3B). Lymphocytes and macrophages appeared mostly unaffected.

Next, we optimized dose regimen. We tested two injections at 3, 10 and 30 μ g/kg given a day apart on day 1 and day 2. No obvious increase in efficacy was observed (S4 Fig). A direct comparison in the same experimental cohort confirmed that there was no statistical difference with 3 μ g/kg given on day 1 only, day 2 only, or day 1 and 2 (Fig 3C and 3D).

Histopathology confirmed that 10 μ g/kg 833c&Freso administered on day 2 protects the lung tissue from bleomycin-induced inflammatory cell influx. After three days bleomycin caused obvious pneumonitis with rampant inflammatory cell infiltration in the tissue interstitium and alveolar air spaces as well as protein exudates and alveolar septal thickening (compare Fig 4A and 4B to 4E normal). These pneumonitis hallmarks [43] were ameliorated by treatment (Fig 4C and 4D). Lung injury scoring quantified the robust bleomycin effect (0.1 ± 0.2 control vs 3.2 ± 0.3 bleomycin) and its 41% inhibition by TGF- β blockade (1.9 ± 0.2 bleomycin plus 833c&Freso) (Fig 4F). In agreement, other experiments independently showed 833c&Freso reduced lung edema from bleomycin by 36%, as assessed by lung wet to dry ratios (Fig 4G).

Our literature search identified 12 well-known biomarkers of related lung diseases [18, 44–48], also induced by bleomycin [49], that we could readily and directly measure as proteins in

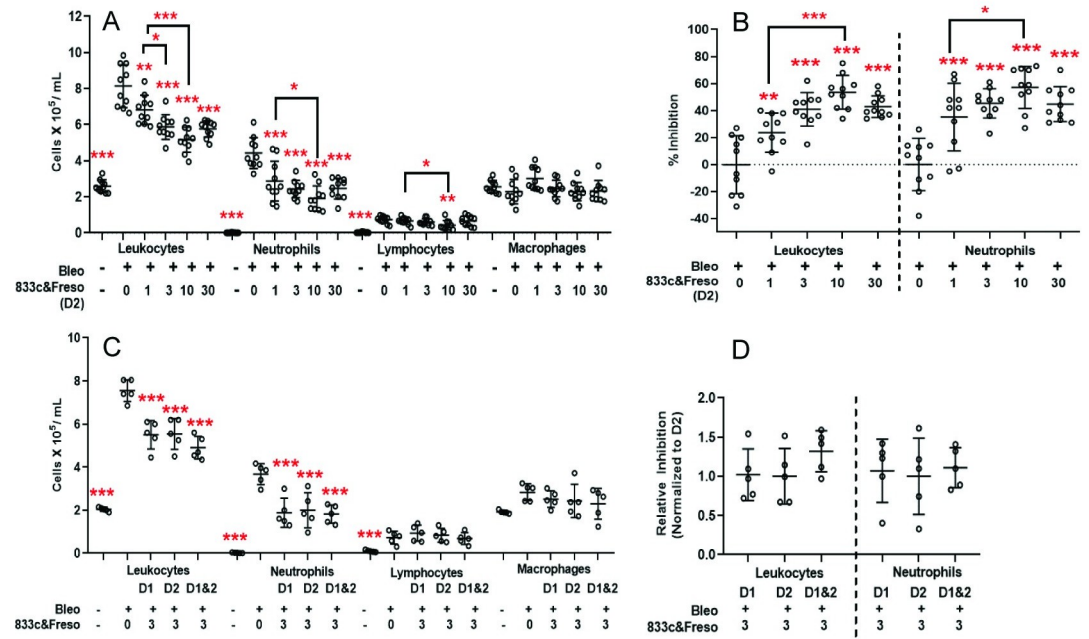


Fig 3. Therapeutic effects of 833c&Freso on bleomycin-induced lung infiltration of inflammatory cells detected in BALf. 833c&Freso at the indicated doses (µg/kg) was injected iv into rats on the indicated days after bleomycin challenge (A–D) day 2 (D2), (C–D) day 1 (D1), (C–D) day 1 and 2 (D1&2)). BALf was collected on day 3. Total leukocyte and neutrophil count per ml of BALf (A,C) and percentage inhibition of the bleomycin effect on total leukocyte and neutrophil infiltration (B). Data pooled from 2 independent experiments totaling n = 10 rats per group. (D) Relative inhibition is normalized to single treatment on D2, with n = 5 rats per group. Scatter graphs showing each data point with indicated means ± SD. *P < 0.03, **P < 0.01, and ***P < 0.001 vs. bleo only, by using one-way ANOVA followed by Dunnett’s test, except as indicated otherwise (A and B) when comparing dose differences with Student’s unpaired t test.

<https://doi.org/10.1371/journal.pone.0276462.g003>

BALf or whole lung homogenates from rats, using commercially available reagents. Although TGF-β1 levels appeared unaffected, 10 µg/kg 833c&Freso significantly decreased the bleomycin-induced signal in BALf for key interleukins, IL-6 (39%) and IL-1β (54%) (Fig 5A); both are inflammatory cytokines regulated by TGF-β [50, 51] and induced by bleomycin [52]. WISP-1, a well-known TGF-β downstream target [53] implicated in fibrogenesis [54], as well as the neutrophil chemoattractant CINC-1 and TIMP-1, a metalloproteinase inhibitor implicated in acute lung injury and tissue remodeling [55], were each reduced by 38%, 68% and 36%, respectively (Fig 5A).

Western blot analysis of lung tissue homogenates confirmed ample TGF-β neutralization preventing receptor engagement by showing significant inhibition of phosphorylation of Smad 2/3 (60%) (Fig 5B and 5C), a well-known immediate consequence of engaged TGF-β receptor kinase activity [31]. Also, galectin-3, an important regulator of fibrosis and activator of neutrophil mobility [56, 57] was downregulated by 49% (Fig 5B and 5C). Fibronectin expression, which likely reflects an early inflammatory remodeling phase [58], was downregulated over 80% with 833c&Freso treatment (Fig 5B and 5C). We did not see any significant blocking of the PI3K/AKT or mTOR signaling pathways or PDGFRβ (S5 Fig) [59].

To elucidate key mechanisms and features of the bispecific antibody required to achieve ultra-low dose efficacy, we similarly tested the therapeutic capabilities of 833c, 833cX&Freso and Freso (Fig 6A–6C). Neither lung-targeting 833c, which does not carry the therapeutic arm, nor 833cX&Freso, which does not bind to APP2 (Fig 1E), reduced total leukocyte or neutrophil infiltration of BALf at 10 µg/kg doses. Thus, mutating just 2 amino acids in the 833c

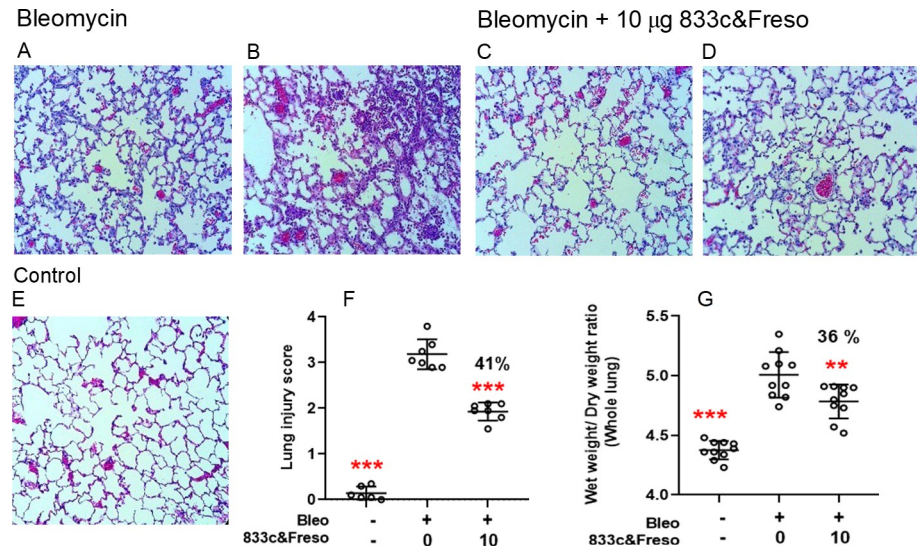


Fig 4. Therapeutic effect of 833c&Freso on lung pathology and edema from bleomycin. Rats were treated with 10 µg/kg 833c&Freso iv on day 2 after bleomycin challenge. Lungs excised on day 3 were sectioned and stained with H&E. Light microscopy images (×20) showing lung histopathology (A–D) vs. normal (E). Tissue damage was clearly evident but varied within each group, ranging from low (A, C) to high (B, D). (F) Lung damage in each 20x microscopy field was scored as described in Methods. (G) Wet to dry lung weight ratio, n = 10 total rats per group. Scatter graphs indicate means ± SD. Percentage (%) inhibition of lung injury scores (F) and edema (G) is indicated. **P < 0.01, and *** P < 0.001 were obtained vs bleo control by one-way ANOVA followed by Dunnett’s test.

<https://doi.org/10.1371/journal.pone.0276462.g004>

heavy chain CDR region of the bispecific antibody abolished its APP2 reactivity (Fig 1E), its lung targeting (Fig 2C and 2D) and its low dose therapeutic potency (Fig 6A–6D), while SEC profiles (S1 Fig) as well as TGF-β binding (Fig 1F) were maintained. In a separate experiment to rule out possible dual target therapeutic synergy, we also did not detect any infiltration reduction when 833c and fresolimumab were injected together at 10 µg/kg each (S6 Fig) whereas 833c&Freso worked well again, indicating that fusion of the two antibodies was essential for therapeutic efficacy. Ultimately antibody binding to APP2 appears to increase potency here not as a direct therapeutic target but rather indirectly as a delivery target mediating caveolae transcytotic pumping into the lung.

Fresolimumab also failed at 10 µg/kg dose as well as at 1 mg/kg (Fig 6). It required 3 mg/kg to obtain a statistically significant inhibitory effect (Fig 6A–6D). Note the ≥1000-fold increase in potency of 833c&Freso (µg/kg) compared to fresolimumab (mg/kg) (Fig 6E and 6F). Together these data show that targeted drug delivery via APP2 pumping is required to generate a pronounced therapeutic effect for fresolimumab at µg/kg doses. This precision active lung delivery enables ultra-low dose TGF-β antibody efficacy.

With 70–80% of this novel heterobifunctional therapeutic delivered to the lung in 1 h, caveolae pumping achieves ~10 times the maximum blood concentration inside the lung (~10 nM with 10 µg/kg dose). This rapid uptake and concentrating effect, even against an opposing concentration gradient, is consistent with active transport (pumping) into the lung by caveolae. This level inside lung tissue is well above the low nM affinity of the therapeutic arm of the bispecific, fresolimumab. This maximizes immunobinding that neutralizes TGF-β effector functions. Without enough free TGF-β to activate its receptors and downstream signaling, such as Smad phosphorylation (Fig 5B and 5C), TGF-β’s role in inflammation, edema and biomarkers is inhibited. A 3 µg/kg dose yields near but likely still above Kd concentration, thereby

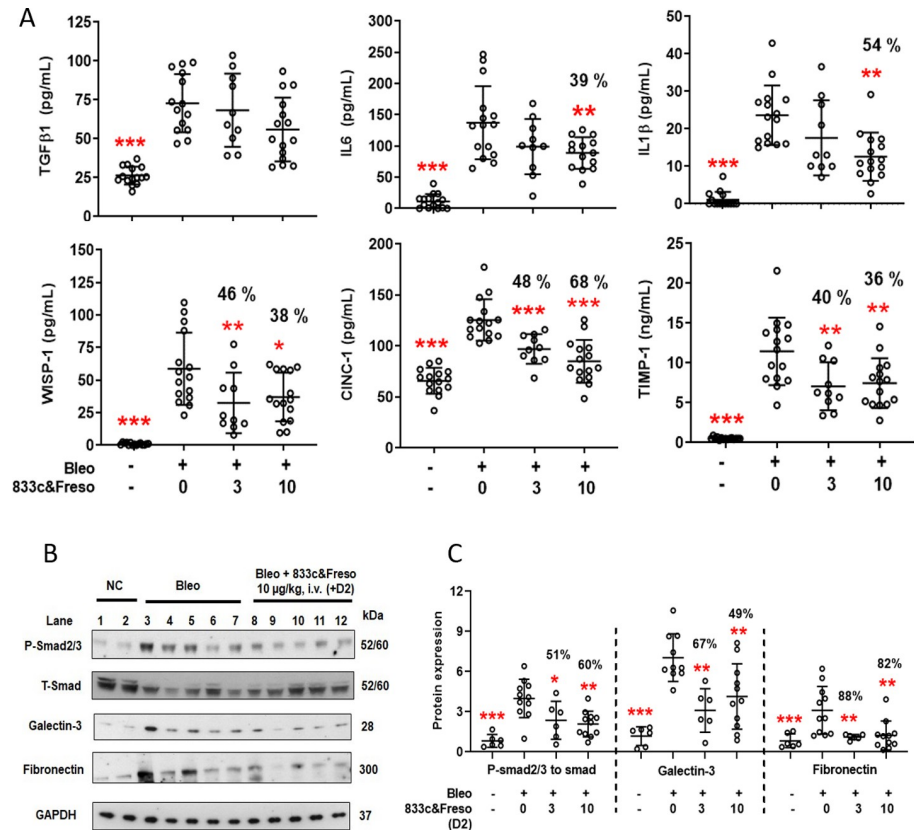


Fig 5. 833c&Freso reduces TGF-β-mediated disease biomarkers and signaling in the lung. Biochemical assays were performed on lung samples taken from untreated rats and rats treated as indicated with 833c&Freso on day 2 after bleomycin challenge. BALf or lung tissue was harvested on day 3. (A) Concentration of the indicated biomarkers detected in BALf. Data pooled from 2–3 independent experiments with n = 10–15 total rats per group. (B) Western blot of lung tissue homogenates using antibodies to the indicated proteins. GAPDH: loading control. Data pooled from 2–3 independent experiments with n = 6–11 total rats per group. (C) Relative expression of indicated proteins derived from western blot image analysis. Smad 2/3 protein phosphorylation: ratio of P- to T Smad 2/3. Graphs show means ± SD. Percentage (%) inhibition of biomarkers in BALf (A) and proteins expressed in the lung (C) are shown. *P < 0.03, **P < 0.01, and *** P < 0.001 were obtained vs bleo control by one-way ANOVA followed by Dunnett’s test.

<https://doi.org/10.1371/journal.pone.0276462.g005>

blocking most but not all TGF-β. Our data appear internally self consistent and readily explain why 1 μg/kg but not 3 μg/kg was found statistically less effective than 10 μg/kg.

Fresolimumab on the other hand requires 3 mg/kg iv dose to achieve therapeutic activity (Fig 6). Peak blood levels of ~300 nM at this dose appear to be needed to drive low nM concentrations required inside the lung to block enough TGF-β to render therapeutic efficacy akin to that observed with the bispecific antibody at 1 μg/kg (Fig 6). Passive transvascular delivery of antibody appears to require at least a 100-fold concentration gradient across the EC barrier to drive enough inside tissue to be effective. In contrast, active transcytosis of APP2 antibody actually creates a gradient in the opposite direction where lung concentrations exceed even peak blood levels (Fig 2) [7]. This study exposes just how limiting the EC barrier can be. We discover by overcoming it so readily that the EC barrier in lungs is no longer just theoretical in its impact but rather quite formidable and exigent in limiting Ab uptake and efficacy, even at high doses. With subnM levels in the blood from low μg/kg doses, immunotargeting caveolae pumping achieves therapeutic nM lung concentrations only attainable passively at mg/kg doses. Up to this point the endothelium has been limiting and appeared “unfriendly” to

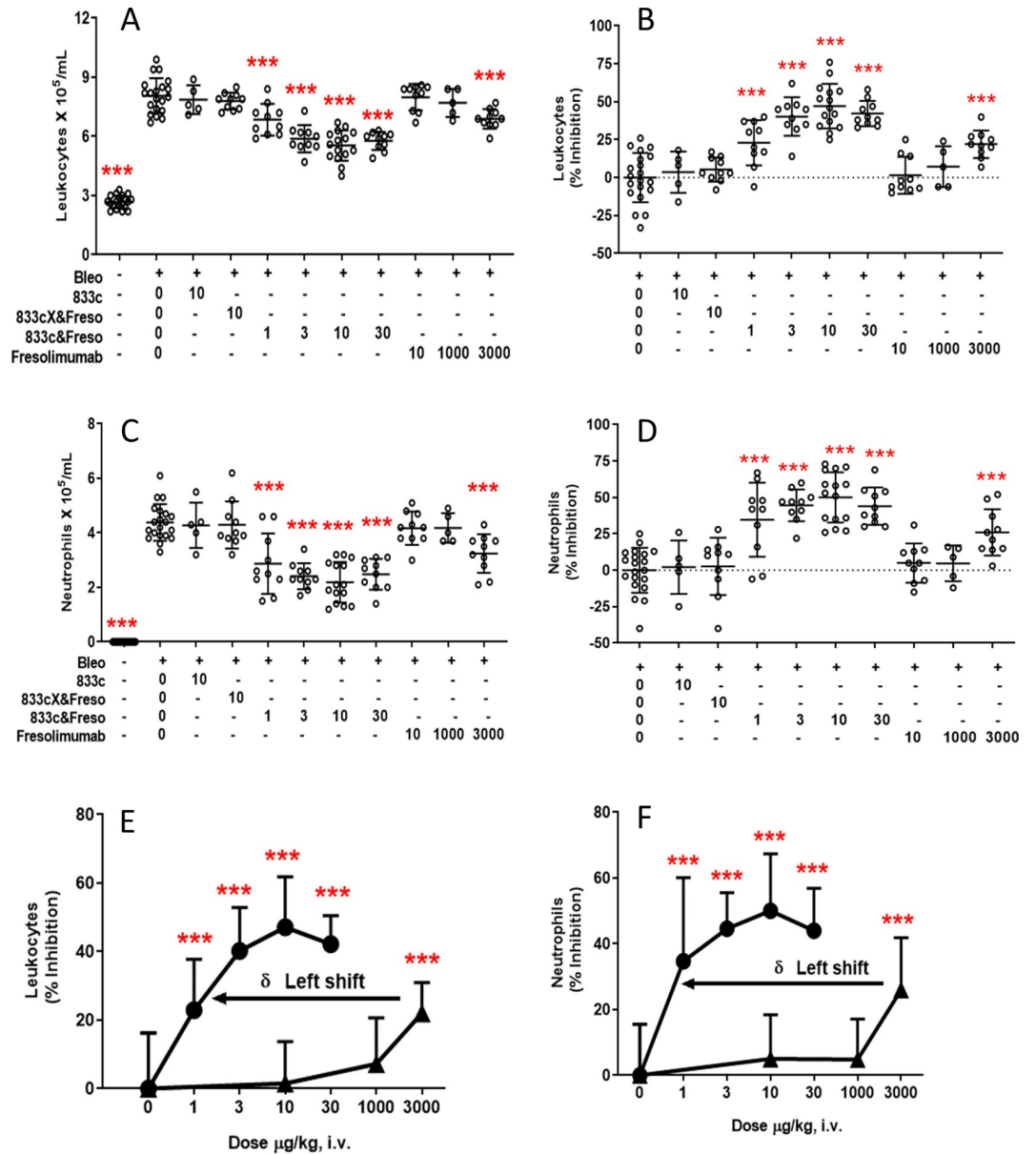


Fig 6. Lung targeting increases therapeutic potency of TGF-β blockade. Two days after bleomycin exposure, rats were treated iv with 833c, 833cX&Freso, 833c&Freso, or fresolimumab at the indicated doses (μg/kg). BALf was collected on day 3. Total leukocytes (A) and neutrophils (C) per ml of BALf. Percent (%) inhibition of leukocyte (B,E) and neutrophil (D,F) accumulation in BALf. (E,F) 833c&Freso (solid circles), fresolimumab (solid triangles). Graphs and statistical analysis as in Fig 3. Data were pooled from 1 to 4 independent experiments with n = 5–20 rats per group.

<https://doi.org/10.1371/journal.pone.0276462.g006>

therapy, but now, for the first time, the endothelium through caveolae mediated pumping can be a facilitator promoting therapeutic potency and efficacy.

Discussion

Like other targets, targeting moieties, and drug delivery pathways and systems discovered with great theoretical promise, our discovery of APP2 and the caveolae pumping system in lung requires stringent, quantitative testing in diseased settings to assess any possible therapeutic

benefit. We have begun to report here critical proofs of principle validating the caveolae-mediated drug delivery strategy by retargeting an already exquisitely precise therapeutic drug, the TGF β blocking antibody fresolimumab. We show that caveolae pumping in the vascular endothelium can still function well in pneumonitis and that caveolae can pump therapeutic antibody into diseased lung to achieve unprecedented precision therapeutic targeting and efficacy, all at strikingly low doses. We have created the first bispecific antibody or other drug that after systemic administration precisely targets inside a single, normally restrictive solid tissue to exert therapeutic efficacy at microdoses. It is engineered to be precisely and actively delivered by caveolae only across the microvascular endothelium in lung tissue. Transendothelial pumping from the blood rapidly concentrates it to levels well above its affinity to help maximize target TGF- β blockade inside the diseased lung tissue and thereby boost its anti-inflammatory potency.

Precision therapeutics are extraordinary in their high affinity and molecular specificity at low concentrations but frequently not in their targeting once injected intravenously. Our therapeutic prototype is the first to be administered systemically (iv bolus) at therapeutic dosages commensurate to the drug's binding affinity to its target (nM) rather than 2 or more orders of magnitude in excess. High affinity precision antibodies attempting to treat diseases inside a solid tissue usually require μ M blood levels attained from standard therapeutic doses of 10 mg/kg or more. The blood levels for small molecule precision therapeutics can easily be 100-fold higher, despite again nM or better affinities. Blood levels near or below 1 nM have never yielded solid tissue targeting and therapeutic efficacy as described herein. That is because passive drug delivery into a tissue with a sufficiently restrictive EC barrier cannot attain interstitial concentrations rivaling or exceeding blood maximums. Passive extravasation is driven not by transcytotic pumping but rather primarily the maximum concentration in the blood which dissipates readily. The caveolae pumping system can continue to transport in a direction opposite to the concentration gradient and thus boosts interstitial concentrations to an order of magnitude above blood levels, all within minutes of iv injection.

Our findings here represent a major advance for therapeutic antibodies, bispecific and in general, towards greater utility and impact in solid tissues with EC barriers limiting passive extravasation. The lung restricts entry and microdose therapeutic efficacy until fresolimumab is re-engineered into a bispecific format enabling retargeting to the caveolae pumping system in lung microvascular endothelium. Once injected iv to circulate in the blood, the two delivery arms of the bispecific antibody have inherent access to its intended EC delivery target in caveolae for active and rapid extravasation to the lung interstitium. Now the two precision therapeutic arms have rapidly attained unprecedented target access so that TGF- β can be comprehensively engaged at high, near saturation concentrations and functionally blocked to abate inflammation at lower doses. The APP2 concentrated in caveolae on the luminal EC surface only in lung microvessels is critical to the precision lung targeting, tissue penetration and concentration process. Without APP2 binding, active drug delivery to lung is lost and so is the dual precision therapeutic efficacy at extraordinarily low μ g/kg doses. Standard passive drug delivery ensues and remains limited to requiring >1000-fold higher doses to achieve any efficacy with fresolimumab alone. The precision therapeutic on its own can't perform optimally without active delivery across the restrictive endothelial barrier.

Getting 70–80% of injected dose into a single solid tissue of the therapeutic antibody or for that matter any drug is remarkable; to do so within 1 hr even more so. Small molecules extravasate passively better than antibodies to bind targets inside restrictive tissues but still have not targeted with such precision, speed, extent and low dosage as 833c&Freso. Usurping physiological pumping mechanisms can concentrate key radioactive small molecules like iodine in thyroid even at low doses but rapid renal filtration excretes the vast majority after iv injection.

High affinity ligand-mimicking peptides can bind physiological receptors to accumulate in a few endocrine and tumor tissues but require high blood levels (μM) that dissipate within minutes due to rapid renal elimination [60, 61]. Moreover, unlike many past studies reporting pre-clinical testing of mono-, bi- and tri-specific antibodies including some reaching clinical trials [62, 63], all results here occur under native *in vivo* conditions with only endogenous target expression levels and are devoid of any target and/or species-specific manipulations rendering favor to the desired delivery and therapeutic outcome. Active transvascular delivery can indeed enable precision targeting well beyond passive delivery.

Here we show active delivery by targeting caveolae-mediated transcytosis in lung improves precision targeting by >100-fold which leads to even greater enhancement in precision therapeutic potency. Targeting and therapeutic goals near theoretical expectations can be achieved with a bispecific antibody at nM concentrations - all to the benefit of avoiding toxicities. Furthermore, the rapid blood clearance (~80% in 1hr) not from metabolism or renal excretion but rather robust uptake in a single desired target tissue minimizes exposure and toxicities elsewhere in the body.

Although representing a major step forward towards achieving “magic bullet” utility, this study uses only a single therapeutic construct in one disease model. This study and the caveolae-mediated drug delivery paradigm in general have many unaddressed issues and possible limitations. Establishing broader utility in other lung diseases awaits further study. Some pathologies may more directly affect endothelial cell function to possibly disable caveolae pumping. Whether caveolae targeting works in other organs, normal and diseased, requires more target discovery. Also, the bispecific format used here is limited; it is only one of many and provides only two blocking opportunities per molecule. Loading antibodies with small inhibitors either directly via chemical conjugation or indirectly for instance by attaching drug nanocarriers, may provide more impact. Utilizing antibody derivatives and other targeting agents to study the effects of size, affinity, avidity, drug loading and nanoparticles on caveolae pumping and precision tissue targeting may even provide further insights and improvements beyond an already prodigious start. So far, we do not detect any evidence of interference by target presence in circulating blood, for instance from APP2 shedding and/or TGF- β secretion. In human serum, TGF- β is sequestered and functionally inactive in the blood protein alpha-2 macroglobulin [64]. However, this could become potentially limiting in other pathologies.

This new approach provides the first benefits bestowed through a new active drug delivery paradigm; a means to penetrate the EC barrier that has plagued delivery into many normal and diseased tissues/organs; a means to more readily and fully engage therapeutic targets usually hidden inside so many organs. We have created a new class of “dual precision” medicine by coupling two specific antibodies, one providing unprecedented lung delivery, the other exclusive therapeutic target neutralization. The result is a highly specific molecular therapeutic agent that elevates the *in vivo* pharmacological potency by 3 orders of magnitude directly by solving the delivery problem. Lung targeting via caveolae appears paramount to achieve the marked therapeutic effect of 833c&Freso at $\mu\text{g}/\text{kg}$ doses.

We ultimately demonstrate the therapeutic value of accurate single tissue drug delivery and penetration. Overcoming the EC barrier through caveolae pumping may be key to maximizing therapeutic impact and eliminating ambiguity as to cause when a drug fails. If delivery is assured, then the drug’s pharmacological activity can be maximized to yield efficacy commensurate with the target effector’s role in the disease. Dual delivery and therapeutic precision targeting encourages a paradigm shift from passive to active drug delivery; accordingly therapeutic drug doses may drop from mg/kg to $\mu\text{g}/\text{kg}$. Many drugs may benefit from similar targeted caveolae pumping, especially drugs showing promising activity yet limited by high dose toxicities, sometimes even leading to failed clinical trials. This novel delivery strategy

could expand our applicable drug repertoire and ultimately revolutionize treatment options, if successful in clinical trials.

Supporting information

S1 Fig. Size-exclusion chromatogram with multi angle light scattering detection of 833c, fresolimumab, 833c&Freso and 833cX&Freso. Average hydrodynamic radius (nm):

833c = 5.2, fresolimumab = 5.0, 833c&Freso = 6.1, and 833Xc&Freso = 6.1.

(TIF)

S2 Fig. Prophylactic effect of 833c&Freso on inflammatory cells in bronchoalveolar fluid (BALf). Rats were treated with 833c&Freso at the indicated doses ($\mu\text{g}/\text{kg}$) by iv injection one hour before (-1 h) administering bleomycin (bleo) it (see [Methods](#)). BALf was collected on day 3. **(A)** Total and differential leukocyte concentrations in BALf. **(B)** Percent (%) inhibition of total leukocyte and neutrophil infiltration. Data were pooled from 2 independent experiments with 833c&Freso 10 $\mu\text{g}/\text{kg}$ repeated in both experiments ($n = 4\text{--}9$ total rats per group). Scatter graphs of each data point are shown with indicated means \pm SD. * $P < 0.03$, ** $P < 0.01$, and *** $P < 0.001$ vs. bleo only, by using one-way ANOVA followed by Dunnett's test.

(TIF)

S3 Fig. TGF- β expression in bleomycin challenged rats. Rats received a single it instillation of bleomycin as described in [Methods](#). BALf was collected and TGF- β 1 concentration determined by ELISA. *** $P < 0.001$ vs day 0, by using one way ANOVA followed by Dunnett's test.

(TIF)

S4 Fig. Dose optimization of 833c&Freso. Rats were injected with 833c&Freso at the indicated doses ($\mu\text{g}/\text{kg}$) on day 1 and day 2 (D1&2) after bleomycin (bleo) exposure. BALf was collected on day 3. **(A)** Total and differential leukocyte profile in BALf. **(B)** Relative cell numbers normalized to 10 $\mu\text{g}/\text{kg}$. Data pooled from 1–4 independent experiments with $n = 5\text{--}22$ total rats per group. Scatter graphs of each data point with indicated means \pm SD. * $P < 0.03$, ** $P < 0.01$, and *** $P < 0.001$ vs. bleo only, by using one-way ANOVA followed by Dunnett's test.

(TIF)

S5 Fig. 833c&Freso does not affect PDGF/AKT/mTOR axis signaling in the lung. Rats were treated with 10 $\mu\text{g}/\text{kg}$ 833c&Freso iv on day 2 post-bleomycin. Lung tissue was harvested on day 3. **(A)** Lung tissue homogenates were subjected to western blot analysis using antibodies to indicated proteins. **(B)** Relative expression of PDGFR β , P-AKT to AKT and P-p70S6K to p70S6K derived from western blot image analysis. Scatter graphs of each data point with indicated means \pm SD. $N = 3\text{--}5$ rats per group. *** $P < 0.001$ vs. bleo only, by using one-way ANOVA followed by Dunnett's test.

(TIF)

S6 Fig. 833c plus fresolimumab does not affect leukocyte and neutrophil infiltration. Rats were injected with either 10 $\mu\text{g}/\text{kg}$ of 833c and fresolimumab or 10 μg 833c&Freso on day 2 after bleomycin (bleo) exposure. BALf was collected on day 3. **(A)** Total leukocyte and neutrophils in BALf. **(B)** Percentage (%) inhibition of leukocyte and neutrophil infiltration. $N = 4$ rats per group. Scatter graphs of each data point with indicated means \pm SD. * $P < 0.03$, ** $P < 0.01$, and *** $P < 0.001$ vs. bleo only, by using one-way ANOVA followed by Dunnett's test.

(TIF)

S1 Raw images.

(PDF)

S2 Raw images.
(PDF)

S3 Raw images.
(PDF)

Author Contributions

Conceptualization: Anil H. Kadam, Jan E. Schnitzer.

Funding acquisition: Zea Borok, Jan E. Schnitzer.

Investigation: Anil H. Kadam, Kathirvel Kandasamy, Tim Buss, Brittany Cederstrom, Chun Yang, Sreekanth Narayanapillai, Juan Rodriguez.

Methodology: Anil H. Kadam, Kathirvel Kandasamy, Tim Buss, Brittany Cederstrom, Chun Yang, Michael D. Levin, Jim Koziol, Bogdan Olenyuk, Adrian Chrastina, Jan E. Schnitzer.

Validation: Jim Koziol.

Writing – original draft: Anil H. Kadam, Kathirvel Kandasamy, Jan E. Schnitzer.

Writing – review & editing: Zea Borok, Jan E. Schnitzer.

References

1. Strebhardt K, Ullrich A. Paul Ehrlich's magic bullet concept: 100 years of progress. *Nature reviews*. 2008; 8(6):473–80. <https://doi.org/10.1038/nrc2394> PMID: 18469827
2. Manzari MT, Shamay Y, Kiguchi H, Rosen N, Scaltriti M, Heller DA. Targeted drug delivery strategies for precision medicines. *Nature Reviews Materials*. 2021; 6(4):351–70. <https://doi.org/10.1038/s41578-020-00269-6> PMID: 34950512
3. Bae YH, Park K. Advanced drug delivery 2020 and beyond: perspectives on the future. *Advanced drug delivery reviews*. 2020; 158:4–16. <https://doi.org/10.1016/j.addr.2020.06.018> PMID: 32592727
4. Glassman PM, Myerson JW, Ferguson LT, Kiseleva RY, Shuvaev VV, Brenner JS, et al. Targeting drug delivery in the vascular system: focus on endothelium. *Advanced drug delivery reviews*. 2020; 157:96–117. <https://doi.org/10.1016/j.addr.2020.06.013> PMID: 32579890
5. Schnitzer JE. Update on the cellular and molecular basis of capillary permeability. *Trends in Cardiovasc Med*. 1993; 3:124–30. [https://doi.org/10.1016/1050-1738\(93\)90012-U](https://doi.org/10.1016/1050-1738(93)90012-U) PMID: 21244938
6. Kim SM, Faix PH, Schnitzer JE. Overcoming key biological barriers to cancer drug delivery and efficacy. *J Control Release*. 2017; 267:15–30. <https://doi.org/10.1016/j.jconrel.2017.09.016> PMID: 28917530
7. Oh P, Borgstrom P, Witkiewicz H, Li Y, Borgstrom BJ, Chrastina A, et al. Live dynamic imaging of caveolae pumping targeted antibody rapidly and specifically across endothelium in the lung. *Nat Biotechnol*. 2007; 25(3):327–37. <https://doi.org/10.1038/nbt1292> PMID: 17334358
8. Oh P, Li Y, Yu JY, Durr E, Krasinska KM, Carver LA, et al. Subtractive proteomic mapping of the endothelial surface in lung and solid tumours for tissue-specific therapy. *Nature*. 2004; 429(6992):629–35. <https://doi.org/10.1038/nature02580> PMID: 15190345
9. Oh P, Testa JE, Borgstrom P, Witkiewicz H, Li Y, Schnitzer JE. In vivo proteomic imaging analysis of caveolae reveals pumping system to penetrate solid tumors. *Nature medicine*. 2014; 20(9):1062–8. <https://doi.org/10.1038/nm.3623> PMID: 25129480
10. Chrastina A, Valadon P, Massey KA, Schnitzer JE. Lung vascular targeting using antibody to aminopeptidase P: CT-SPECT imaging, biodistribution and pharmacokinetic analysis. *Journal of vascular research*. 2010; 47(6):531–43. <https://doi.org/10.1159/000313880> PMID: 20431301
11. Schnitzer JE, Liu J, Oh P. Endothelial caveolae have the molecular transport machinery for vesicle budding, docking, and fusion including VAMP, NSF, SNAP, annexins, and GTPases. *J Biol Chem*. 1995; 270(24):14399–404. <https://doi.org/10.1074/jbc.270.24.14399> PMID: 7782301
12. Schnitzer JE, Allard J, Oh P. NEM inhibits transcytosis, endocytosis, and capillary permeability: implication of caveolae fusion in endothelia. *Am J Physiol*. 1995; 268(1 Pt 2):H48–55.

13. Oh P, McIntosh DP, Schnitzer JE. Dynamin at the neck of caveolae mediates their budding to form transport vesicles by GTP-driven fission from the plasma membrane of endothelium. *J Cell Biol.* 1998; 141(1):101–14. <https://doi.org/10.1083/jcb.141.1.101> PMID: 9531551
14. Schnitzer JE. The endothelial cell surface and caveolae in health and disease. In: Born GVR, Schwartz CJ, editors. *Vascular Endothelium: Physiology, pathology and therapeutic opportunities.* Stuttgart: Schattauer; 1997. p. 77–95.
15. Schnitzer JE, Oh P, Jacobson BS, Dvorak AM. Caveolin-enriched caveolae purified from endothelium in situ are transport vesicles for albumin-mediated transcytosis of albumin. *Mol Biol Cell.* 1994; 5:A75.
16. Pittet JF, Griffiths MJ, Geiser T, Kaminski N, Dalton SL, Huang X, et al. TGF-beta is a critical mediator of acute lung injury. *J Clin Invest.* 2001; 107(12):1537–44. <https://doi.org/10.1172/JCI11963> PMID: 11413161
17. Peters DM, Vadasz I, Wujak L, Wygrecka M, Olschewski A, Becker C, et al. TGF-beta directs trafficking of the epithelial sodium channel ENaC which has implications for ion and fluid transport in acute lung injury. *Proc Natl Acad Sci U S A.* 2014; 111(3):E374–83.
18. Fahy RJ, Lichtenberger F, McKeegan CB, Nuovo GJ, Marsh CB, Wewers MD. The acute respiratory distress syndrome: a role for transforming growth factor-beta 1. *Am J Respir Cell Mol Biol.* 2003; 28(4):499–503. <https://doi.org/10.1165/rcmb.2002-0092OC> PMID: 12654639
19. Sheppard D. Transforming growth factor beta: a central modulator of pulmonary and airway inflammation and fibrosis. *Proceedings of the American Thoracic Society.* 2006; 3(5):413–7. <https://doi.org/10.1513/pats.200601-008AW> PMID: 16799084
20. Willis BC, Borok Z. TGF-beta-induced EMT: mechanisms and implications for fibrotic lung disease. *Am J Physiol Lung Cell Mol Physiol.* 2007; 293(3):L525–34. <https://doi.org/10.1152/ajplung.00163.2007> PMID: 17631612
21. Deng S, Zhang H, Han W, Guo C, Deng C. Transforming growth factor-beta-neutralizing antibodies improve alveolarization in the oxygen-exposed newborn mouse lung. *J Interferon Cytokine Res.* 2019; 39(2):106–16.
22. Nakanishi H, Sugiura T, Streisand JB, Lonning SM, Roberts JD Jr. TGF-beta-neutralizing antibodies improve pulmonary alveologenesis and vasculogenesis in the injured newborn lung. *Am J Physiol Lung Cell Mol Physiol.* 2007; 293(1):L151–61. <https://doi.org/10.1152/ajplung.00389.2006> PMID: 17400601
23. Prashanth Goud M, Bale S, Pulivendala G, Godugu C. Therapeutic effects of nimbolide, an autophagy regulator, in ameliorating pulmonary fibrosis through attenuation of TGF-beta1 driven epithelial-to-mesenchymal transition. *Int Immunopharmacol.* 2019; 75:105755.
24. Anscher MS, Thrasher B, Rabbani Z, Teicher B, Vujaskovic Z. Antitransforming growth factor-beta antibody 1D11 ameliorates normal tissue damage caused by high-dose radiation. *Int J Radiat Oncol Biol Phys.* 2006; 65(3):876–81. <https://doi.org/10.1016/j.ijrobp.2006.02.051> PMID: 16751069
25. George PM, Wells AU, Jenkins RG. Pulmonary fibrosis and COVID-19: the potential role for antifibrotic therapy. *Lancet Respir Med.* 2020; 8(8):807–15. [https://doi.org/10.1016/S2213-2600\(20\)30225-3](https://doi.org/10.1016/S2213-2600(20)30225-3) PMID: 32422178
26. Zhao X, Nicholls JM, Chen YG. Severe acute respiratory syndrome-associated coronavirus nucleocapsid protein interacts with Smad3 and modulates transforming growth factor-beta signaling. *J Biol Chem.* 2008; 283(6):3272–80. <https://doi.org/10.1074/jbc.M708033200> PMID: 18055455
27. Carvacho I, Piesche M. RGD-binding integrins and TGF-beta in SARS-CoV-2 infections—novel targets to treat COVID-19 patients? *Clin Transl Immunology.* 2021; 10(3):e1240.
28. Shen WX, Luo RC, Wang JQ, Chen ZS. Features of cytokine storm identified by distinguishing clinical manifestations in COVID-19. *Front Public Health.* 2021; 9:671788. <https://doi.org/10.3389/fpubh.2021.671788> PMID: 34109148
29. Mitra MS, Lancaster K, Adedeji AO, Palanisamy GS, Dave RA, Zhong F, et al. A potent pan-TGFbeta neutralizing monoclonal antibody elicits cardiovascular toxicity in mice and cynomolgus monkeys. *Toxicol Sci.* 2020; 175(1):24–34.
30. Ask K, Martin GE, Kolb M, Gauldie J. Targeting genes for treatment in idiopathic pulmonary fibrosis: challenges and opportunities, promises and pitfalls. *Proceedings of the American Thoracic Society.* 2006; 3(4):389–93. <https://doi.org/10.1513/pats.200602-021TK> PMID: 16738206
31. Akhurst RJ. Targeting TGF-beta signaling for therapeutic gain. *Cold Spring Harb Perspect Biol.* 2017; 9(10).
32. Teixeira AF, ten Dijke P, Zhu H-J. On-target anti-TGF-β therapies are not succeeding in clinical cancer treatments: what are remaining challenges? *Frontiers in Cell and Developmental Biology.* 2020; 8(605).
33. Kubiczкова L, Sedlarikova L, Hajek R, Sevcikova S. TGF-beta—an excellent servant but a bad master. *J Transl Med.* 2012; 10:183.

34. Ashcroft T, Simpson JM, Timbrell V. Simple method of estimating severity of pulmonary fibrosis on a numerical scale. *J Clin Pathol*. 1988; 41(4):467–70. <https://doi.org/10.1136/jcp.41.4.467> PMID: 3366935
35. Elder ASF, Bersten AD, Saccone GTP, Bonder CS, Dixon DL. Prevention and amelioration of rodent ventilation-induced lung injury with either prophylactic or therapeutic feG administration. *Lung*. 2019; 197(5):671–80. <https://doi.org/10.1007/s00408-019-00252-1> PMID: 31300872
36. Rhee CK, Lee SH, Yoon HK, Kim SC, Lee SY, Kwon SS, et al. Effect of nilotinib on bleomycin-induced acute lung injury and pulmonary fibrosis in mice. *Respiration*. 2011; 82(3):273–87. <https://doi.org/10.1159/000327719> PMID: 21659722
37. d’Ettorre G, Gentilini Cacciola E, Santinelli L, De Girolamo G, Spagnolello O, Russo A, et al. Covid-19 sequelae in working age patients: A systematic review. *J Med Virol*. 2021. <https://doi.org/10.1002/jmv.27399> PMID: 34655247
38. Jackson MR, Stevenson K, Chahal SK, Curley E, Finney GE, Gutierrez-Quintana R, et al. Low-dose lung radiation therapy for COVID-19 lung disease: a preclinical efficacy study in a bleomycin model of pneumonitis. *Int J Radiat Oncol Biol Phys*. 2021.
39. Nagarajah J, Janssen M, Hetkamp P, Jentzen W. Iodine symporter targeting with (124)I/(131)I theranostics. *J Nucl Med*. 2017; 58(Suppl 2):34s–8s. <https://doi.org/10.2967/jnumed.116.186866> PMID: 28864610
40. Coker RK, Laurent GJ, Shahzeidi S, Lympany PA, du Bois RM, Jeffery PK, et al. Transforming growth factors-beta 1, -beta 2, and -beta 3 stimulate fibroblast procollagen production in vitro but are differentially expressed during bleomycin-induced lung fibrosis. *Am J Pathol*. 1997; 150(3):981–91. PMID: 9060836
41. Moulin A, Mathieu M, Lawrence C, Bigelow R, Levine M, Hamel C, et al. Structures of a pan-specific antagonist antibody complexed to different isoforms of TGFbeta reveal structural plasticity of antibody-antigen interactions. *Protein Sci*. 2014; 23(12):1698–707.
42. Grutter C, Wilkinson T, Turner R, Podichetty S, Finch D, McCourt M, et al. A cytokine-neutralizing antibody as a structural mimetic of 2 receptor interactions. *Proc Natl Acad Sci U S A*. 2008; 105(51):20251–6. <https://doi.org/10.1073/pnas.0807200106> PMID: 19073914
43. Gilhodes JC, Jule Y, Kreuz S, Stierstorfer B, Stiller D, Wollin L. Quantification of pulmonary fibrosis in a bleomycin mouse model using automated histological image analysis. *PLoS One*. 2017; 12(1): e0170561. <https://doi.org/10.1371/journal.pone.0170561> PMID: 28107543
44. Cross LJ, Matthay MA. Biomarkers in acute lung injury: insights into the pathogenesis of acute lung injury. *Crit Care Clin*. 2011; 27(2):355–77. <https://doi.org/10.1016/j.ccc.2010.12.005> PMID: 21440206
45. Manicone AM. Role of the pulmonary epithelium and inflammatory signals in acute lung injury. *Expert Rev Clin Immunol*. 2009; 5(1):63–75. <https://doi.org/10.1586/177666X.5.1.63> PMID: 19885383
46. Wesselkamper SC, Case LM, Henning LN, Borchers MT, Tichelaar JW, Mason JM, et al. Gene expression changes during the development of acute lung injury: role of transforming growth factor beta. *Am J Respir Crit Care Med*. 2005; 172(11):1399–411. <https://doi.org/10.1164/rccm.200502-286OC> PMID: 16100012
47. Goldman JL, Sammani S, Kempf C, Saadat L, Letsiou E, Wang T, et al. Pleiotropic effects of interleukin-6 in a “two-hit” murine model of acute respiratory distress syndrome. *Pulm Circ*. 2014; 4(2):280–8. <https://doi.org/10.1086/675991> PMID: 25006447
48. Olman MA, White KE, Ware LB, Simmons WL, Benveniste EN, Zhu S, et al. Pulmonary edema fluid from patients with early lung injury stimulates fibroblast proliferation through IL-1 beta-induced IL-6 expression. *J Immunol*. 2004; 172(4):2668–77. <https://doi.org/10.4049/jimmunol.172.4.2668> PMID: 14764742
49. Saito F, Tasaka S, Inoue K, Miyamoto K, Nakano Y, Ogawa Y, et al. Role of interleukin-6 in bleomycin-induced lung inflammatory changes in mice. *Am J Respir Cell Mol Biol*. 2008; 38(5):566–71. <https://doi.org/10.1165/rcmb.2007-0299OC> PMID: 18096870
50. Wiegertjes R, van Caam A, van Beuningen H, Koenders M, van Lent P, van der Kraan P, et al. TGF-β dampens IL-6 signaling in articular chondrocytes by decreasing IL-6 receptor expression. *Osteoarthritis and cartilage / OARS, Osteoarthritis Research Society*. 2019; 27(8):1197–207. <https://doi.org/10.1016/j.joca.2019.04.014> PMID: 31054955
51. Bodo M, Carinci P, Baroni T, Bellucci C, Giammarioli M, Pezzetti F, et al. Role of growth factors on extracellular matrix production by chick embryo fibroblasts in vitro. Antagonist effect of TGF-beta through the control of IL-1 and IL-1Ra secretion. *Cytokine*. 1998; 10(5):353–60. <https://doi.org/10.1006/cyto.1997.0301> PMID: 9619373
52. Chaudhary NI, Schnapp A, Park JE. Pharmacologic differentiation of inflammation and fibrosis in the rat bleomycin model. *Am J Respir Crit Care Med*. 2006; 173(7):769–76. <https://doi.org/10.1164/rccm.200505-717OC> PMID: 16415276

53. Klee S, Lehmann M, Wagner DE, Baarsma HA, Königshoff M. WISP1 mediates IL-6-dependent proliferation in primary human lung fibroblasts. *Sci Rep.* 2016; 6:20547. <https://doi.org/10.1038/srep20547> PMID: 26867691
54. Königshoff M, Kramer M, Balsara N, Wilhelm J, Amarie OV, Jahn A, et al. WNT1-inducible signaling protein-1 mediates pulmonary fibrosis in mice and is upregulated in humans with idiopathic pulmonary fibrosis. *J Clin Invest.* 2009; 119(4):772–87. <https://doi.org/10.1172/JCI33950> PMID: 19287097
55. Allen JR, Ge L, Huang Y, Brauer R, Parimon T, Cassel SL, et al. TIMP-1 promotes the immune response in influenza-induced acute lung injury. *Lung.* 2018; 196(6):737–43. <https://doi.org/10.1007/s00408-018-0154-2> PMID: 30167842
56. Snarr BD, St-Pierre G, Ralph B, Lehoux M, Sato Y, Rancourt A, et al. Galectin-3 enhances neutrophil motility and extravasation into the airways during *Aspergillus fumigatus* infection. *PLoS Pathog.* 2020; 16(8):e1008741. <https://doi.org/10.1371/journal.ppat.1008741> PMID: 32750085
57. Robinson BS, Arthur CM, Evavold B, Roback E, Kamili NA, Stowell CS, et al. The sweet-side of leukocytes: galectins as master regulators of neutrophil function. *Front Immunol.* 2019; 10:1762. <https://doi.org/10.3389/fimmu.2019.01762> PMID: 31440233
58. Hernnas J, Nettelblad O, Bjermer L, Sarnstrand B, Malmstrom A, Hallgren R. Alveolar accumulation of fibronectin and hyaluronan precedes bleomycin-induced pulmonary fibrosis in the rat. *Eur Respir J.* 1992; 5(4):404–10. PMID: 1373389
59. Kishi M, Aono Y, Sato S, Koyama K, Azuma M, Abe S, et al. Blockade of platelet-derived growth factor receptor-beta, not receptor-alpha ameliorates bleomycin-induced pulmonary fibrosis in mice. *PLoS One.* 2018; 13(12):e0209786.
60. Kondo E, Iioka H, Saito K. Tumor-homing peptide and its utility for advanced cancer medicine. *Cancer Sci.* 2021; 112(6):2118–25. <https://doi.org/10.1111/cas.14909> PMID: 33793015
61. Sun X, Li Y, Liu T, Li Z, Zhang X, Chen X. Peptide-based imaging agents for cancer detection. *Advanced drug delivery reviews.* 2017;110–111:38–51. <https://doi.org/10.1016/j.addr.2016.06.007> PMID: 27327937
62. Seung E, Xing Z, Wu L, Rao E, Cortez-Retamozo V, Ospina B, et al. A trispecific antibody targeting HER2 and T cells inhibits breast cancer growth via CD4 cells. *Nature.* 2022; 603(7900):328–34. <https://doi.org/10.1038/s41586-022-04439-0> PMID: 35197632
63. Wang S, Chen K, Lei Q, Ma P, Yuan AQ, Zhao Y, et al. The state of the art of bispecific antibodies for treating human malignancies. *EMBO Mol Med.* 2021; 13(9):e14291. <https://doi.org/10.15252/emmm.202114291> PMID: 34431224
64. O'Connor-McCourt MD, Wakefield LM. Latent transforming growth factor-beta in serum. A specific complex with alpha 2-macroglobulin. *J Biol Chem.* 1987; 262(29):14090–9. PMID: 2443501